Research Article | Open Access

Soft Science

Bian *et al. Soft Sci.* **2026**, *6*, 79 **DOI:**10.20517/ss.2026.117

Flexible liver organoid-based assessment of metal–organic framework biocompatibility toward programmable organoid bioengineering

Sumin Bian[1,*], Shixiang Liu[2,3], Hongjie Chi[4,5], Li Chen[2,3], Shiyi Tan[6], Nan Jiang[7,8], Hugo Vankelecom[9], Xuan Zhang[2,3,*], Chenzhong Li[4,5,*]

Keywords:
Liver organoids, metal–organic frameworks, biocompatibility evaluation, programmable nano–bio interfaces, drug delivery, organoid bioengineering

Citation: Bian, S.; Liu, S.; Chi, H.; Chen, L.; Tan, S.; Jiang, N.; Vankelecom, H.; Zhang, X.; Li, C. Flexible liver organoid-based assessment of metal–organic framework biocompatibility toward programmable organoid bioengineering. *Soft Sci.* **2026**, *6*, 79. https://dx.doi.org/10.20517/ss.2026.117

Received: 21 May 2026 **First Decision:** 22 Jun 2026 **Revised:** 13 Jul 2026 **Accepted:** 28 Jul 2026 **Published:** 18 Aug 2026

Academic Editor: Nae-Eung Lee
Copy Editor: Pei-Yun Wang
Production Editor: Pei-Yun Wang

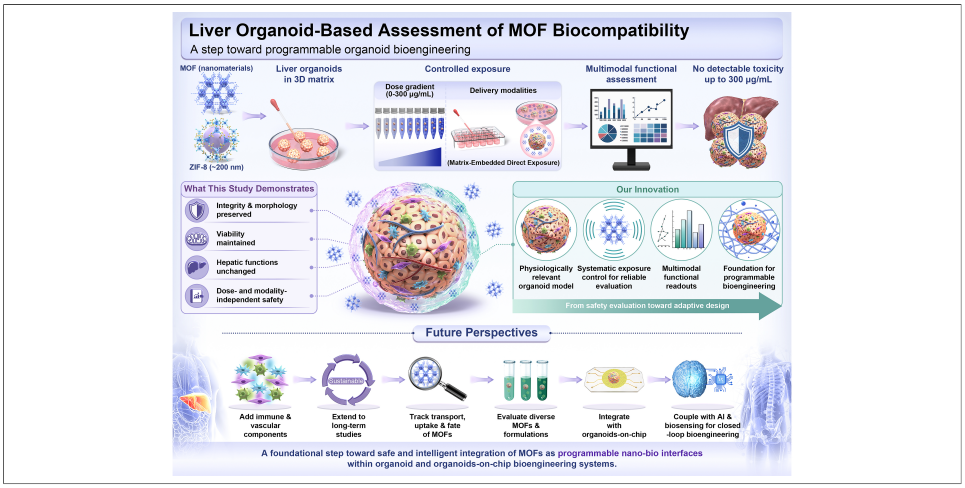

Abstract

Metal–organic frameworks (MOFs) are emerging as versatile nanomaterials for biomedical applications owing to their high surface area, tunable porosity, and structural flexibility. However, concerns regarding their biocompatibility and hepatotoxicity, particularly as applications expand from drug delivery toward emerging bioengineering systems, necessitate physiologically relevant platforms for nanotoxicity evaluation. Here, we establish a liver organoid platform for controlled assessment of MOF biocompatibility. Liver organoids derived from hepatic progenitor cells exhibited hepatic characteristics, including hepatocyte marker expression and robust metabolic activity. Using this platform, we systematically evaluated zeolitic imidazolate framework-8 (ZIF-8), one of the most extensively studied MOFs for drug delivery, under defined exposure conditions using a Matrigel-embedded approach across multiple concentration gradients. Across tested concentrations, ZIF-8 caused no detectable changes in organoid morphology and viability.

[1]Department of Electronic and Information Engineering, School of Engineering, Westlake University, Hangzhou 310030, Zhejiang, China.
[2]School of Materials Science and Engineering, Zhejiang University, Hangzhou 310027, Zhejiang, China.
[3]Advanced Nano-Micro Energy Storage Research Laboratory, ZJU-Hangzhou Global Scientific and Technological Innovation Center, Zhejiang University, Hangzhou 311215, Zhejiang, China.
[4]School of Medicine, The Chinese University of Hong Kong (Shenzhen), Shenzhen 518172, Guangdong, China.
[5]Guangdong Basic Research Center of Excellence for Aggregate Science, School of Science and Engineering, The Chinese University of Hong Kong (Shenzhen), Shenzhen 518172, Guangdong, China.
[6]Key Laboratory of Environmental Medicine Engineering of Ministry of Education, School of Public Health, Southeast University, Nanjing 210018, Jiangsu, China.
[7]West China School of Basic Medical Sciences & Forensic Medicine, Sichuan University, Chengdu 610041, Sichuan, China.
[8]Institute of Panvascular Biology, JinFeng Laboratory, Chongqing 401329, China.

[9]Laboratory of Tissue Plasticity in Health and Disease, Cluster of Stem Cell and Developmental Biology, Department of Development and Regeneration, KU Leuven (University of Leuven), Leuven 3000, Belgium.

*__Correspondence to:__ Prof. Sumin Bian, Department of Electronic and Information Engineering, School of Engineering, Westlake University, Hangzhou 310030, Zhejiang, China. E-mail: biansumin@westlake.edu.cn; Prof. Xuan Zhang, Advanced Nano-Micro Energy Storage Research Laboratory, ZJU-Hangzhou Global Scientific and Technological Innovation Center, Zhejiang University, Hangzhou 311215, Zhejiang, China. E-mail: xuanzhangzju@zju.edu.cn; Prof. Chenzhong Li, School of Medicine, The Chinese University of Hong Kong (Shenzhen), Shenzhen 518172, Guangdong, China. E-mail: lichenzhong@cuhk.edu.cn

Histological architecture and hepatic function at representative concentrations were confirmed by hematoxylin and eosin staining, and alanine aminotransferase, aspartate aminotransferase, urea, and albumin analyses. Collectively, these findings demonstrate no detectable toxicity at concentrations up to 300 μg/mL under the investigated conditions over 96 h in a physiologically relevant organoid model. Importantly, this proof-of-concept study demonstrates the feasibility of using liver organoids as physiologically relevant platforms for ZIF-8 biocompatibility assessment, supporting multimodal functional readouts and controlled exposure conditions. The proposed organoid-based framework may be extended to systematic evaluation of additional MOF systems with diverse physicochemical properties, compositions, and biomedical applications, while facilitating future exploration of MOFs as programmable nano–bio interfaces for organoid and organoid-on-chips bioengineering. The platform may also support future integration with biosensing, artificial intelligence, and closed-loop bioengineering applications.

INTRODUCTION

Metal–organic frameworks (MOFs) are a class of crystalline porous materials formed by the coordination of metal ions or clusters with organic ligands[1]. Owing to their exceptional structural tunability and physicochemical properties[2-4], MOFs enable precise control over pore size, shape, surface chemistry, and framework flexibility through the selection of metal centers, ligands, and synthesis strategies[5]. These features yield ultra-high specific surface area, tunable adsorption performance, and excellent optical and electrical properties[6-10]. Recently, nanoscale MOFs have emerged as particularly promising platforms for biosensing[11,12], drug delivery, and broader biomedical applications[13,14]. Among them, zeolitic imidazolate framework-8 (ZIF-8) is one of the most extensively investigated MOFs for drug delivery owing to its high porosity, large drug-loading capacity, and pH-responsive degradation, making systematic biocompatibility evaluation essential for its safe biomedical translation[15,16]. Their nanoscale dimensions confer favorable pharmacokinetic properties, including enhanced cellular uptake and improved tissue penetration, making them especially suitable for therapeutic use[15,16].

Compared to conventional drug delivery systems, MOFs offer modular and tunable architectures that enable precise control over morphology, composition, particle size, and surface functionalities[17]. The stimuli-responsive behavior of MOFs may also represent a form of embedded programmability, enabling conditional and spatiotemporally controlled modulation of organoid microenvironments in response to cues such as pH, glutathione, ionic strength, temperature, magnetic fields, and mechanical forces[18-23]. In addition, their high specific surface area and intrinsic porosity provide abundant internal space for efficient drug encapsulation[24]. Dynamic coordination bonds may confer biodegradability, an essential feature for safe and effective biomedical applications[25].

Beyond their well-established role as drug delivery carriers, MOFs are increasingly explored as functional nanomaterials for bioengineering applications[26]. In particular, their tunable porosity, chemical versatility, and stimuli-responsive behavior make them attractive candidates for integration into three-dimensional (3D) biological systems, including organoids and organoid-on-chips (OOC). In this context, MOFs may function not only as delivery vehicles but also as nano–bio interfaces capable of localized delivery, microenvironment modulation, and dynamic regulation of biochemical cues[27]. These capabilities support

the development of adaptive organoid and OOC systems with improved control over spatiotemporal microenvironmental signals and enhanced predictive power of *in vitro* models[28].

This dual functionality introduces a critical need to reassess MOF biocompatibility from two complementary perspectives. First, as nanocarriers for drug delivery, where systemic safety is essential for clinical translation because MOF toxicity is often concentration-dependent[24,29]. Second, as potential components of organoid and OOC bioengineering systems, including microenvironment modulation, advanced cultivation strategies, and cryopreservation[30,31]. Therefore, evaluating MOF nanotoxicity in physiologically relevant organoid systems is a necessary step toward both safe nanomedicine development and the future integration of nanomaterials into engineered living systems.

Advanced 3D *in vitro* models, particularly organoids and OOC systems, have recently emerged as transformative tools in drug toxicity assessment[32,33]. Compared with 2D cultures and animal models, organoids more faithfully reproduce the 3D architecture, cellular heterogeneity, and functionality of human organs, enabling more accurate predictions of drug behavior and toxicity *in vivo*[34,35]. In addition, organoids retain donor-specific genetic and epigenetic features, allowing for the identification of inter-individual variability in drug response[36,37]. This makes them particularly valuable in the context of personalized and precision medicine, and of organ toxicology. Among organ-specific models, liver organoids are especially promising for evaluating the toxicity of emerging materials such as MOFs. The liver plays a central role in xenobiotic metabolism and is often a primary target for systemic toxicity[38]. Liver organoids recapitulate key hepatic functions, including drug metabolism, bile secretion, and inflammatory signaling. Unlike hepatocyte cultures, they maintain long-term viability and liver-specific gene expression[39], supporting chronic exposure studies.

Building on our previous work - where we developed microelectromechanical system-based sensing arrays for comparative *in vitro* nanotoxicity assessment at the single-cell level[40], and explored the feasibility of OOCs for modeling neural diseases[41] - the present study advances this line of research by investigating the hepatotoxic effects of MOFs using liver organoids. This physiologically relevant model enables more precise evaluation of MOF-induced cellular responses and facilitates early detection of potential safety risks. By integrating organoid-based toxicological assessment with material design, our approach supports the rational development of MOF-based biomedical applications while proactively addressing critical safety concerns. While the present study focuses on ZIF-8 as a representative MOF and a liver organoid model, it is intended as a proof-of-concept demonstration of organoid-based biocompatibility assessment rather than a comprehensive evaluation of MOF families. Future studies involving additional MOF systems, organoid models, and exposure conditions will be required to establish the broader applicability of the proposed framework.

EXPERIMENTAL

Materials

$Zn(NO_3)_2·6H_2O$ (99%) was supplied by Alfa Aesar (China) Chemical Co., Ltd. 2-methylimidazole (HMIM, 98%) and sodium formate (99.99%) were purchased from Macklin Biochemical Co., Ltd. The liver organoid culture system utilizes a comprehensive set of reagents including progenitor and differentiation media (MasterAim, 100-469, 100-498, 100-499; Hangzhou AimingMed Technologies Co., Ltd., Hangzhou, China), Matrigel (Corning, 356231), and cell handling supplements such as Y-27632 (MCE, HY-10071), anti-adhesion solution (MasterAim 100-291; Hangzhou AimingMed Technologies Co., Ltd., Hangzhou, China), TrypLE (Gibco, 12604021), and Dulbecco's Phosphate-Buffered Saline (DPBS, Gibco, 14190114). Organoid harvesting and RNA extraction are supported by Cell Recovery Solution (Corning, 354253) and Trizol Reagent (Invitrogen, 15596018CN), followed by gene expression analysis using the PrimeScript RT Reagent

Kit (Takara Bio Inc., Shiga, Japan; RR036A) and TB Green Premix Ex Taq II (Takara Bio Inc., Shiga, Japan; RR420A). Histological assessment is conducted with hematoxylin and eosin (H&E) staining reagents (Servicebio G1004 and G1001), while functional assays include alanine aminotransferase (ALT/GPT) and aspartate aminotransferase (AST/GOT) kits (ADS-W-AJS001-96, ADS-W-AJS002-96; Jiangsu Aidisheng Biotechnology Co., Ltd., China), as well as urea, albumin (elabscience, E-BC-K329-S, E-BC-K057-M; Elabscience Biotechnology Inc., Wuhan, China), and CellTiter-Glo® luminescent cell viability assay (Promega, Madison, WI, USA; G7573). Single-donor human serum off-the-clot and single-donor human urine were commercially purchased from Innovative Research (Shanghai, China).

Key equipment used includes a CO_2 incubator (371GP, Thermo Fisher Scientific) for cell culture, inverted and upright microscopes [Axio Observer 7 inverted microscope (Carl Zeiss AG, Oberkochen, Germany) and Axiolab 5 upright microscope (Carl Zeiss AG, Oberkochen, Germany)] for morphological assessment, and a full-spectrum microplate reader a Varioskan LUX multimode microplate reader (Thermo Fisher Scientific, Waltham, MA, USA) for biochemical assays. Histological processing is performed using a paraffin microtome (Leica Biosystems, Wetzlar, Germany), while gene expression is quantified via a QuantStudio 6 Pro Real-Time PCR System (Thermo Fisher Scientific, Waltham, MA, USA). Additional tools include a cell counter Countstar Mira BF (ALIT Life Science Co., Ltd., Shanghai, China) and a LAMBDA 1050 UV/Vis/NIR spectrophotometer (PerkinElmer, Waltham, MA, USA).

MOFs preparation

ZIF-8 nanoparticles were synthesized following a previously reported method with minor modifications[42]. A solution was prepared by dissolving 734.4 mg (2.469 mmol) of $Zn(NO_3)_2{\cdot}6H_2O$ in 50 mL of methanol. Another solution was made by dissolving 810.6 mg (9.874 mmol) of HMIM and 671.5 mg (9.874 mmol) of sodium formate in 50 mL of methanol. The second solution was then added to the first solution under stirring, and the reaction was allowed to proceed at room temperature for 24 h. After the reaction, the precipitate was collected by centrifugation, washed with methanol, and dried at 60 °C in an oven.

Hepatic organoid culture

The hepatic organoids used in this study were generated by differentiating hepatic progenitor cell organoids. These progenitor organoids were originally derived from commercially available human embryonic stem cells (hESCs; H1, Cat No: CL-0889, Wuhan Procell Biotechnology) following a standardized protocol[43] and stored for later use. Prior to experimentation, the frozen hepatic progenitor cell organoids were rapidly thawed at 37 °C, centrifuged at 300 g for 5 min, and then resuspended in Matrigel at a density of 2,000 cells/μL. Fifty-microliter droplets were seeded into pre-warmed 24-well plates and incubated to solidify the matrix. Each well was then supplemented with 800 μL of pre-warmed hepatic organoid culture medium containing 5 μM Y-27632. Organoids were maintained at 37 °C and 5% CO_2 for 3 days to allow recovery, with medium changes every 2-3 days without the addition of Y-27632. Differentiation was then initiated by replacing the culture medium with hepatic differentiation medium, which was refreshed daily. Organoids were passaged during differentiation as required by digesting with TrypLE, centrifugation, resuspension in Matrigel at 500 clusters per 50 μL, and reseeding. Differentiation was continued for 12 days, followed by a 3-day maturation period in complete differentiation medium with daily medium changes, resulting in functionally mature hepatic organoids.

Morphological assessment

On days 0, 15, and 18 following the passage of hepatic progenitor cell organoids (corresponding to hepatic progenitor cell organoids, semi-differentiated hepatic organoids, and mature hepatic organoids, respectively), bright-field images were captured.

Table 1. Primer sequences used for quantitative qPCR analysis

Primer	Primer sequence
β-actin-F	CACCATTGGCAATGAGCGGTTC
β-actin-R	AGGTCTTTGCGGATGTCCACGT
HNF4α-F	GGTGTCCATACGCATCCTTGAC
HNF4α-R	AGCCGCTTGATCTTCCCTGGAT
AFP-F	GCAGAGGAGATGTGCTGGATTG
AFP-R	CGTGGTCAGTTTGCAGCATTCTG
ALB-F	GATGAGATGCCTGCTGACTTGC
ALB-R	CACGACAGAGTAATCAGGATGCC
KRT19-F	AGCTAGAGGTGAAGATCCGCGA
KRT19-R	GCAGGACAATCCTGGAGTTCTC

qPCR: Quantitative polymerase chain reaction.

H&E staining assessment

H&E staining of hepatic organoids begins with tissue sampling and fixation. Liver organoids are first released from Matrigel using cold Cell Recovery Solution, collected gently into adhesive-resistant tubes, and digested on ice for 20-40 min. After sedimentation, the organoids are transferred into a custom-made agar well in an Eppendorf tube. Following gentle centrifugation and removal of the supernatant, molten agar is added to fully embed the organoids. The agar blocks are fixed in paraformaldehyde overnight at 4 °C. Subsequently, the organoid-embedded agar blocks are dehydrated through a graded ethanol series, cleared in xylene, and infiltrated with paraffin using a tissue processor. After embedding in paraffin molds, the solidified blocks are trimmed and sectioned using a microtome. Sections are mounted on slides, baked, and stained sequentially with H&E. After differentiation, bluing, and rinsing, the slides are dehydrated through an ethanol-xylene series and finally mounted with neutral resin for imaging.

Quantitative polymerase chain reaction analysis

Total RNA was extracted from hepatic progenitor cell organoids, and hepatic organoids using TRIzol. Samples were lysed in 0.5 mL TRIzol, mixed with chloroform, and centrifuged to separate phases. The aqueous phase was collected, precipitated with isopropanol, washed with 75% ethanol, air-dried, and resuspended in DEPC water. For reverse transcription, 0.5 μg of RNA was mixed with PrimeScript RT Master Mix and RNase-free water, and incubated at 37 °C for 15 min, followed by 85 °C for 5 s. For quantitative polymerase chain reaction (qPCR), cDNA was combined with TB Green Premix Ex Taq, primers, and water in a 20 μL reaction volume. A two-step qPCR protocol was used to obtain Ct values, and relative gene expression levels were calculated using the $2^{-\Delta\Delta Ct}$ method. Primer sequences are detailed in Table 1 as follows.

Liver function assessment

GPT/ALT assay

To assess GPT/ALT, hepatic progenitor and mature hepatic organoids (~10^6 cells) were collected and lysed in 1 mL of extraction solution using an ultrasonic disruptor (200 W, 3 s on/10 s off, 30 cycles in an ice bath). The lysates were centrifuged at 12,000 rpm for 10 min, and the resulting supernatants were collected and kept on ice. For the assay, standard curves and reaction systems were prepared according to the manufacturer's instructions. The reaction mixture was sequentially incubated with Reagent One at 37 °C for 30 min, Reagent Two at 37 °C for 10 min, and Reagent Three at 25 °C for 10 min. Absorbance was measured at 520 nm. The concentration of the reaction product in the GPT/ALT assay was calculated based on the standard curve and expressed in μM.

GOT/AST assay

Hepatic progenitor and mature hepatic organoids containing approximately 10^6 cells were lysed in 1 mL of extraction solution using an ultrasonic disruptor (200 W, 3 s on/10 s off, 30 cycles in an ice bath). After centrifugation for 10 min, the supernatant was collected and kept on ice. For GOT/AST analysis, standard curves and sample systems were prepared following the manufacturer's protocol. The lysates were sequentially mixed with Reagent One and incubated at 37 °C for 30 min, followed by Reagent Two for an additional 10 min, and finally with Reagent Three at 25 °C for 10 min. Absorbance was measured at 520 nm. The concentration of the reaction product generated in the GOT/AST assay was calculated based on the standard curve and expressed in μM.

Urea production and albumin secretion assay

The supernatant from 24-hour cultures of organoids, maintained at consistent cell densities, was collected for analysis. For the urea production assay, standard curves and sample solutions were prepared according to the manufacturer's instructions. Reagent One and Reagent Two were mixed, incubated at 95 °C for 15 min, then cooled in an ice bath. Absorbance was measured at 520 nm to determine urea concentration. For the albumin secretion assay, Reagent One was first incubated at 25 °C for 10 min, and absorbance was subsequently measured at 630 nm to calculate albumin concentration.

Evaluation of MOF ZIF-8 toxicity

Preparation of ZIF-8 suspension

A ZIF-8 stock solution was prepared by dissolving ZIF-8 in hepatic organoid differentiation medium at a concentration of 1,000 μg/mL, followed by ultrasonic dispersion and sterile filtration. This stock solution was then diluted with the same medium to obtain a series of test concentrations: 300, 250, 200, 150, 100, 50, 25, 10, and 0 μg/mL. These solutions were subsequently used for the Matrigel-embedded administration described in Section "Matrigel ZIF-8 administration".

Matrigel ZIF-8 administration

Following the above procedure, a ZIF-8 stock solution was diluted with hepatic organoid differentiation medium to prepare 3× working solutions at concentrations of 900, 750, 600, 450, 300, 150, 75, 30, and 0 μg/mL, corresponding to final gel concentrations of 300, 250, 200, 150, 100, 50, 25, 10, and 0 μg/mL, respectively. Mature hepatic organoids cultured in a 24-well plate were gently detached using DPBS; the Matrigel was separated from the organoids, and the suspension was centrifuged to remove the supernatant. The organoids were then resuspended, counted, and aliquoted into tubes at 1,500 organoids per tube, followed by another centrifugation step. Each organoid pellet was resuspended in 10 μL of the corresponding 3× ZIF-8 working solution and mixed with 20 μL of Matrigel at a 1:2 volume ratio, resulting in final gel concentrations of 300, 250, 200, 150, 100, 50, 25, 10, and 0 μg/mL. The mixtures were seeded into a 96-well plate at 10 μL per well, resulting in final gel drug concentrations of 300, 250, 200, 150, 100, 50, 25, 10, and 0 μg/mL. After the Matrigel solidified, 0.1 mL of hepatic organoid differentiation medium was added to each well, and the organoids were cultured at 37 °C with 5% CO_2 for 4 days, with daily medium replacement. Bright-field images of the organoids were taken from day 0 to day 4 during the ZIF-8 exposure.

Determination of organoid viability curve after ZIF-8 exposure

To assess organoid viability following ZIF-8 exposure, the 96-well plate was first equilibrated at room temperature for 30 min. Without removing the culture medium, 100 μL of CellTiter-Glo® luminescent cell viability assay reagent was added to each well, followed by gentle agitation and a 2-min incubation to facilitate cell lysis. The resulting lysate was transferred to a non-transparent detection plate, and luminescence was measured using a plate reader. This assay quantifies intracellular adenosine triphosphate

(ATP) levels, serving as a reliable indicator of metabolically active, viable cells. Relative organoid viability (RV%) was calculated using the formula below according to the CellTiter-Glo® Luminescent Cell Viability Assay Technical Manual (Promega). The IC_{50} value of the viability curve was determined using statistical software. Histological staining and liver function assays of organoids after drug exposure were conducted using previously described methods.

$$RV\% = (RLU_{drug\text{-}treated} - RLU_{blank}) / (RLU_{control} - RLU_{blank}) \times 100\%$$

RESULTS AND DISCUSSION

MOFs preparation and characterization

In this study, an effective material synthesis technique was carried out based on our previously developed protocol[42], as briefly described in Figure 1A. As a result, highly uniform and monodispersed rhombic dodecahedral ZIF-8 particles with an average particle size of approximately 200 nm were obtained, as shown in the scanning electron microscopy (SEM) image (Figure 1B: inset image). The well-defined rhombic dodecahedral morphology is consistent with the characteristic crystal habit of ZIF-8 reported in previous studies and indicates successful framework formation. Energy-dispersive X-ray spectroscopy (EDS) qualitatively verified the presence of Zn, C, and N elements in the product. Although EDS is not intended for accurate quantification of light elements such as C and N, the observed elemental signals are consistent with the expected composition of ZIF-8. No obvious impurity-related elemental signals were detected, further supporting the successful synthesis of the target material. Powder X-ray diffraction (PXRD) further confirmed its crystal structure and phase purity [Figure 1C]. The measured PXRD pattern showed excellent agreement with the simulated ZIF-8 diffraction pattern. Characteristic diffraction peaks observed at approximately 7.3°, 10.4°, 12.7°, 14.8°, 16.4°, and 18.0° were consistent with the reported sodalite-type ZIF-8 crystal structure. Furthermore, the absence of additional diffraction peaks indicates high crystallinity and phase purity, with no detectable crystalline impurities or secondary phases. Collectively, these results confirm the successful synthesis of phase-pure ZIF-8 nanoparticles suitable for subsequent biocompatibility evaluation.

Hepatic organoid culture and characterization

The hepatic organoids were generated by differentiating hepatic progenitor cell organoids originally derived from hESCs. The timeline of the study procedure is illustrated in Figure 2A. Briefly, hepatic progenitor organoids were thawed on Day 0 and allowed to recover for 3 days. Differentiation was initiated on Day 3, followed by organoid passaging, maturation, and maintenance until Day 25. Morphological, molecular (qPCR), and functional assessments were performed at key time points. MOF treatment was later initiated on Day 25 and continued until Day 29, after which morphology, cell viability, histology (H&E), and liver function were evaluated.

During culture, hepatic progenitor cell organoids predominantly exhibit a cystic appearance, whereas differentiated hepatic organoids (Days 15-25) develop an increasingly dense, darkened core [Figure 2B]. These differentiated organoids display a thickened and proliferative outer cell layer, with cellular contents accumulating in the lumen. Such morphological changes are consistent with progressive hepatic maturation and increased cellular organization during differentiation. This transition is further supported by H&E staining [Figure 2C]. Hepatic progenitor cell organoids show cytoplasmic vacuolation, and the nuclei are round or nearly round. In contrast, differentiated hepatic organoids exhibit hyperplasia and thickening of the outer cell layer, along with luminal cellular debris and content. The histological changes indicate structural remodeling and the establishment of a more mature tissue-like architecture.

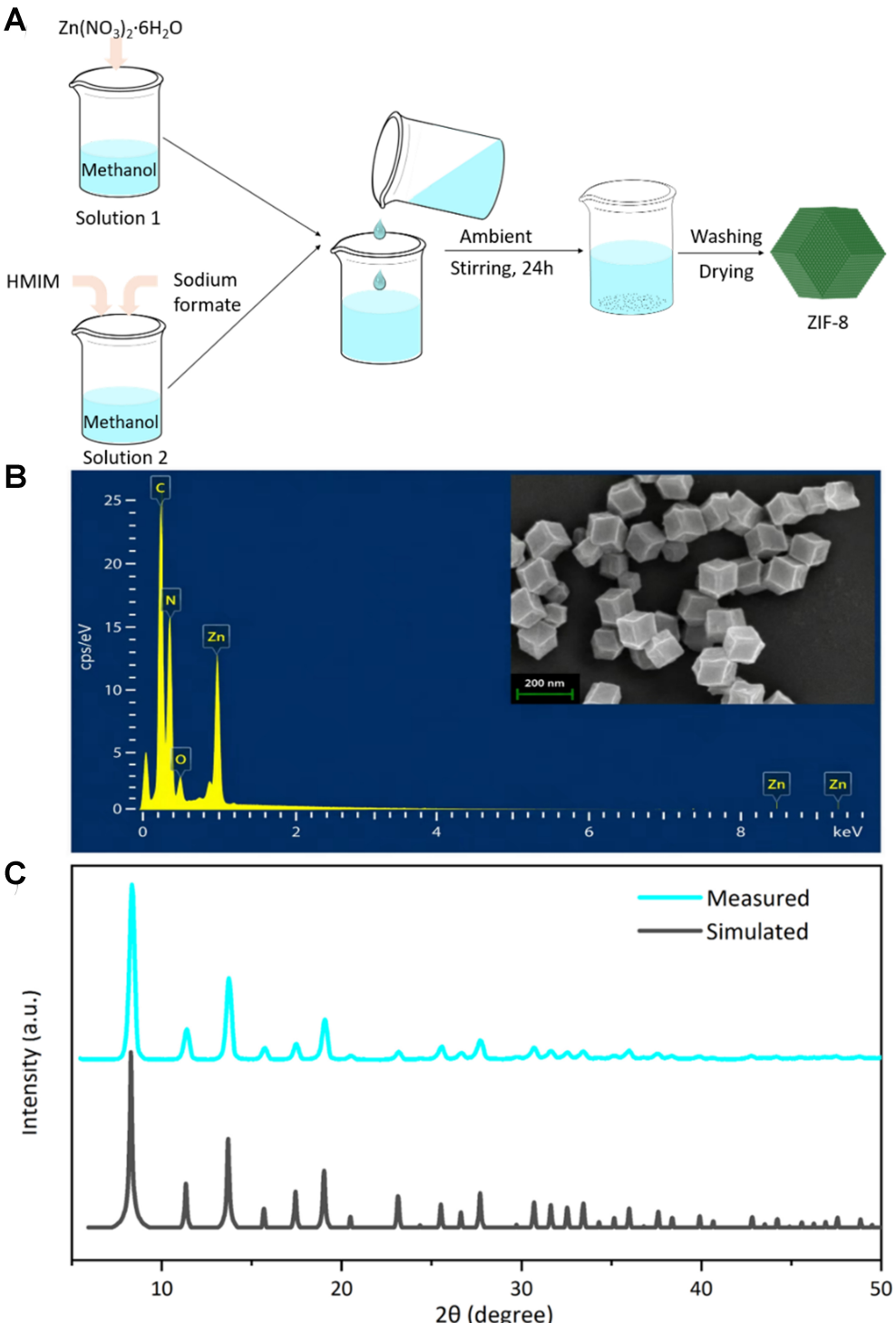

Figure 1. Characterization of the ZIF-8 nanomaterial. (A) Preparation process of ZIF-8; (B) EDS image and the SEM image (inset, with a 200 nm scale bar) of the ZIF-8; (C) PXRD pattern of ZIF-8. ZIF-8: Zeolitic imidazolate framework-8; EDS: energy-dispersive X-ray spectroscopy; SEM: scanning electron microscopy; PXRD: powder X-ray diffraction; HMIM: 2-methylimidazole.

Additionally, qPCR analysis revealed a decrease in the expression of the hepatic progenitor marker gene KRT19 and an increase in hepatocyte-specific markers alpha-fetoprotein (AFP), albumin (ALB), and HNF4α in differentiated organoids compared to progenitor organoids [Figure 2D]. The downregulation of KRT19 together with the upregulation of AFP, ALB, and HNF4α further confirms the transition from a progenitor-like state toward a hepatocyte-like phenotype. Functional assessments also showed increased urea and

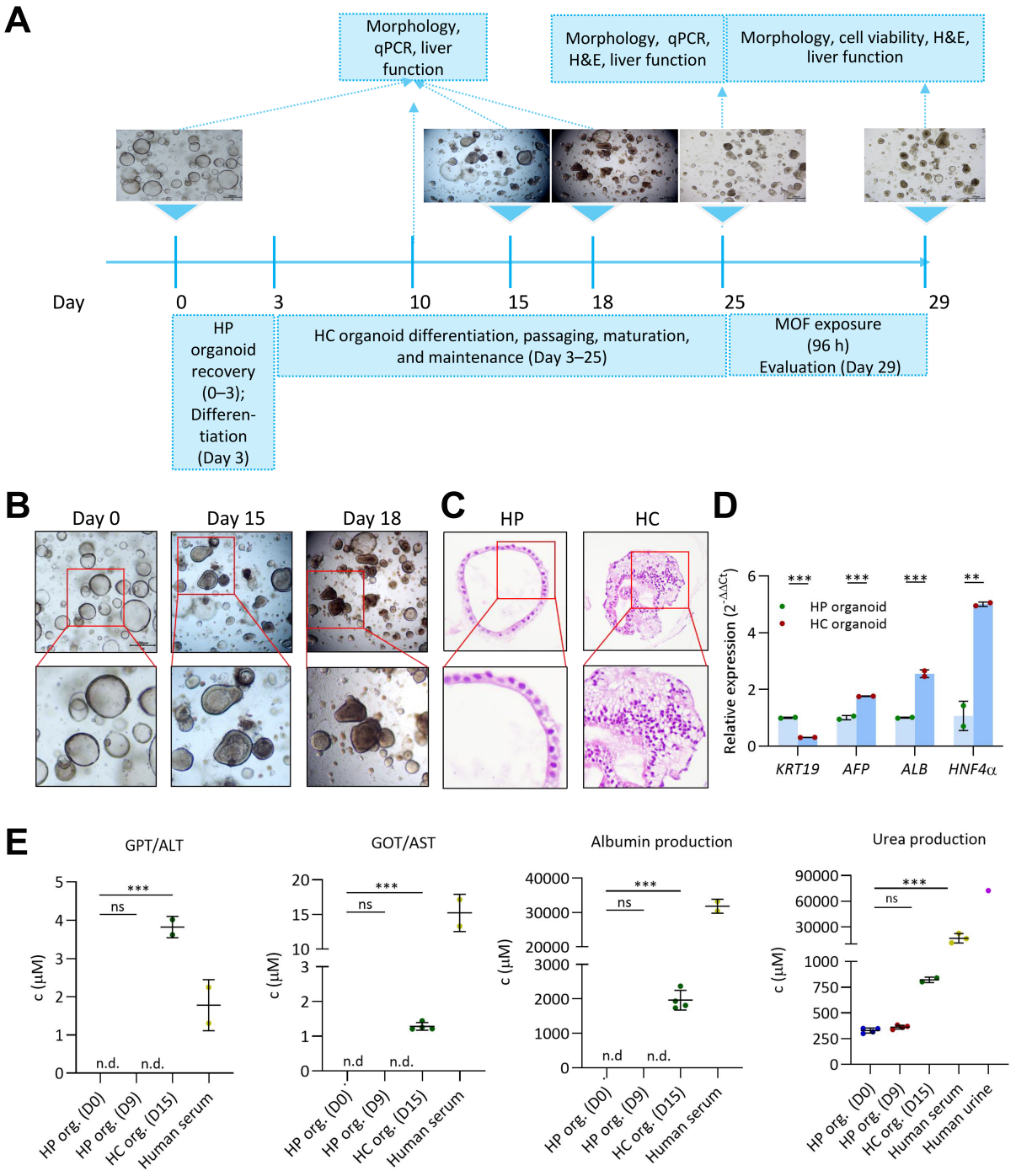

Figure 2. (A) Timeline of liver organoid culture and differentiation and the subsequent exposure; (B-E) Construction and characterization of HP and HC organoids. (B) Bright-field images of the HP organoid (Day 0) and the HC organoids cultured on Day 15 and Day 18, respectively; (C) Histological characterization (H&E staining) and (D) qPCR characterization of HP and differentiated HC organoids; as well as (E) Liver function characterization of HP and differentiated HC organoids. For (D), statistical comparisons between two groups were performed using Student's *t*-test. For (E), multiple-group comparisons were performed using ordinary one-way ANOVA followed by Dunnett's multiple comparisons test, with the corresponding HP group serving as the control. $^{**}P < 0.01$; $^{***}P < 0.001$. All bright-field images were acquired at 4× magnification with a 500 μm scale bar. "ns" indicates not significant ($P > 0.05$). Error bars represent the standard deviation. Data are presented as mean ± SD ($n = 4$ biological replicates, measured values of the original data points). HP: Hepatic progenitor; HC: hepatocyte; H&E: hematoxylin and eosin; qPCR: quantitative polymerase chain reaction; ANOVA: analysis of variance; SD: standard deviation; MOF: metal–organic framework; AFP: alpha-fetoprotein; ALB: albumin; GPT/ALT: alanine aminotransferase; GOT/AST: aspartate aminotransferase.

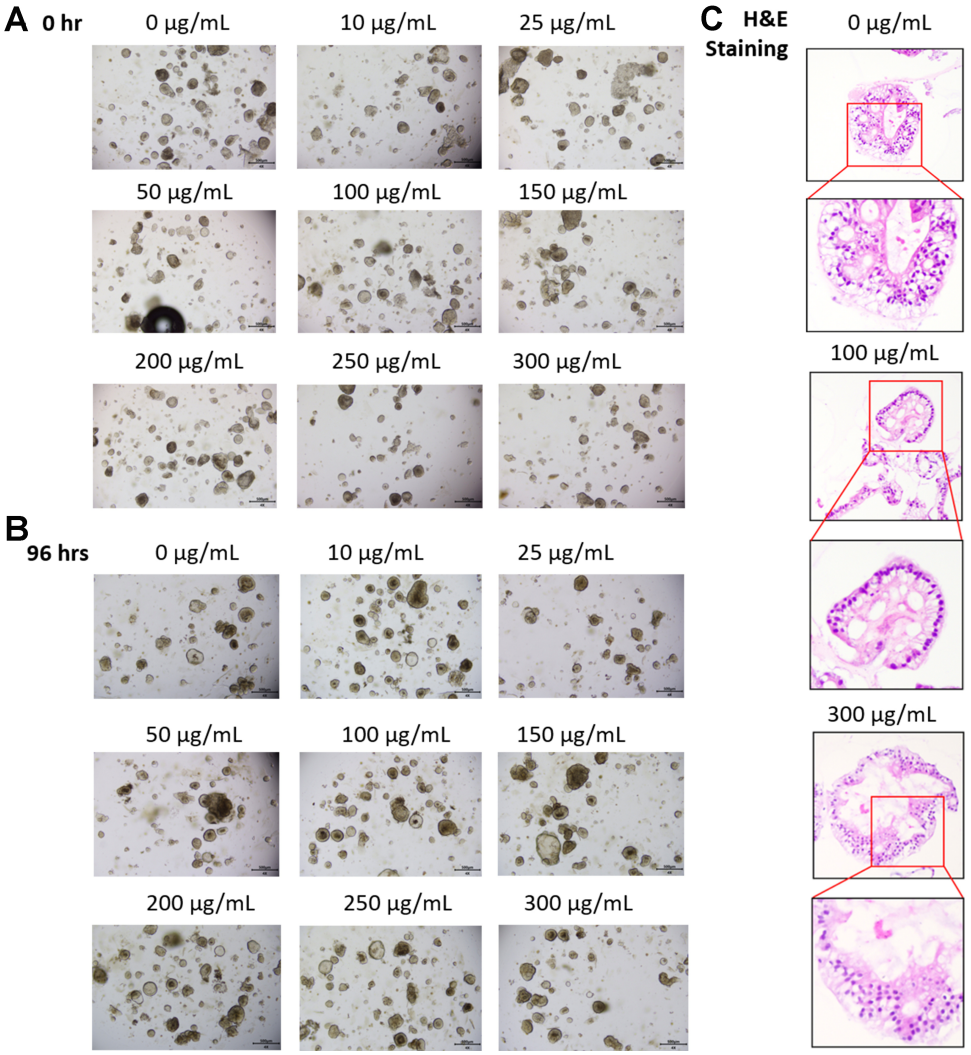

Figure 3. Evaluation of MOF ZIF-8 biocompatibility using hepatic organoids. Hepatic organoids at (A) 0 h and (B) 96 h after a series of ZIF-8 concentration loading; (C) Assessment of the Histological assessment (H&E staining) of hepatic organoids at 96 h after a series of ZIF-8 concentrations. All bright-field images were acquired at 4× magnification with a 500 μm scale bar. MOF: Metal–organic framework; ZIF-8: zeolitic imidazolate framework-8; H&E: hematoxylin and eosin.

albumin production, as well as increased reaction-product concentrations in the ALT and AST assays following differentiation [Figure 2E]. These functional improvements demonstrate enhanced metabolic activity and liver-specific functionality, indicating successful maturation of the hepatic organoids. Collectively, these results confirm the successful differentiation of hepatic progenitor cells into functional hepatocyte organoids.

Evaluation of MOF biocompatibility using hepatic organoids: morphology and characterization

MOF toxicity was evaluated using hepatic organoids from Day 25 to Day 29 (96 h) [Figure 2A]. Morphological aspects were monitored before [Figure 3A] and 96 h after exposure [Figure 3B] to a range of MOF concentrations (0, 10, 25, 50, 100, 150, 200, 250, and 300 μg/mL) administered within the Matrigel. No apparent signs of apoptosis were observed in hepatic organoids within the 96-hour exposure period. Furthermore, no obvious concentration-dependent changes in organoid size, morphology, or structural integrity were detected across the tested concentration range. The organoids maintained their characteristic spherical architecture and cellular organization following exposure to ZIF-8.

H&E staining examination of hepatic organoids [Figure 3C] was performed at 96 h following MOF ZIF-8 administration within the Matrigel at the indicated concentrations. Compared to the control group (0 μg/mL), treatment with medium (100 μg/mL) and high (300 μg/mL) concentrations for 96 h did not result in any notable histological changes in the hepatic organoids. In particular, the overall tissue architecture, epithelial cell layer, and luminal organization remained comparable to those observed in the untreated control group, with no evidence of widespread cell loss, tissue disruption, or necrotic lesions. These observations indicate that the nanomaterial exhibits no hepatotoxicity within the tested range up to 300 μg/mL under the investigated exposure conditions.

Evaluation of MOF biocompatibility using hepatic organoids: viability and liver function

Viability assays conducted 96 h after ZIF-8 administration at a range of concentrations revealed no significant decrease in organoid survival compared to the untreated control group (0 μg/mL), as shown in Figure 4A. Although minor fluctuations in average viability were observed at intermediate concentrations, these variations were within the normal biological and experimental variability of organoid cultures and did not exhibit a concentration-dependent trend. Accordingly, the IC_{50} value was estimated to be greater than 300 μg/mL under the investigated conditions. Collectively, these results indicate that under the investigated exposure conditions, ZIF-8 exhibited no detectable adverse effects on organoid viability and was well tolerated during short-term exposure.

In parallel, liver function analysis, including key metabolic indicators such as GPT/ALT, GOT/AST, albumin secretion, and urea production, showed no measurable impairment following exposure to moderate (100 μg/mL) and high (300 μg/mL) concentrations of ZIF-8, as shown in Figure 4B. No significant differences were observed between control and ZIF-8-exposed groups for any functional readout. Notably, preserved albumin secretion and urea production indicate maintained hepatic metabolic function, while unchanged reaction-product concentrations in the GPT/ALT and GOT/AST assays further support further support the preservation of hepatic function following ZIF-8 exposure. Collectively, these results demonstrate that, under the investigated exposure conditions, ZIF-8 exhibited no detectable hepatotoxicity and was well tolerated by liver organoids. These findings further support the utility of liver organoids as physiologically relevant platforms for evaluating the biocompatibility of emerging MOF-based nanomaterials.

CONCLUSIONS

In this study, we established a physiologically relevant liver organoid platform for evaluating the hepatotoxicity of MOFs, using ZIF-8 as a representative case study. ZIF-8 was selected as a representative MOF to demonstrate the feasibility of the proposed organoid-based biocompatibility assessment platform. Although broader validation using additional MOF families will be required, the present study establishes an initial proof-of-concept for systematic organoid-based evaluation of MOF biocompatibility. The hepatic organoids exhibited key liver-specific functions, including elevated expression of hepatocyte marker genes, sustained metabolic activity, and structural integrity over time. Upon exposure to ZIF-8 at up to 300 μg/mL for 96 h, no significant changes were observed in organoid morphology, viability, or hepatic function. Under the investigated exposure conditions, ZIF-8 exhibited no detectable hepatotoxicity and was well tolerated by liver organoids, supporting its potential as a biocompatible nanocarrier and demonstrating the utility of the platform for systematic nanotoxicity evaluation. This study extends beyond evaluating individual nanomaterials by establishing an initial organoid-based platform for systematic MOF assessment. Importantly, this study highlights the potential of organoids to serve not only as biological models but also as evaluation platforms for nanomaterial assessment. By enabling controlled modulation of exposure parameters, integration of multimodal functional readouts, and compatibility with high-throughput and data-driven workflows, liver organoids can support physiologically relevant nanotoxicity assessment. This perspective aligns with the emerging vision of reconstructing organoids as engineered and tunable biological systems rather than observational models.

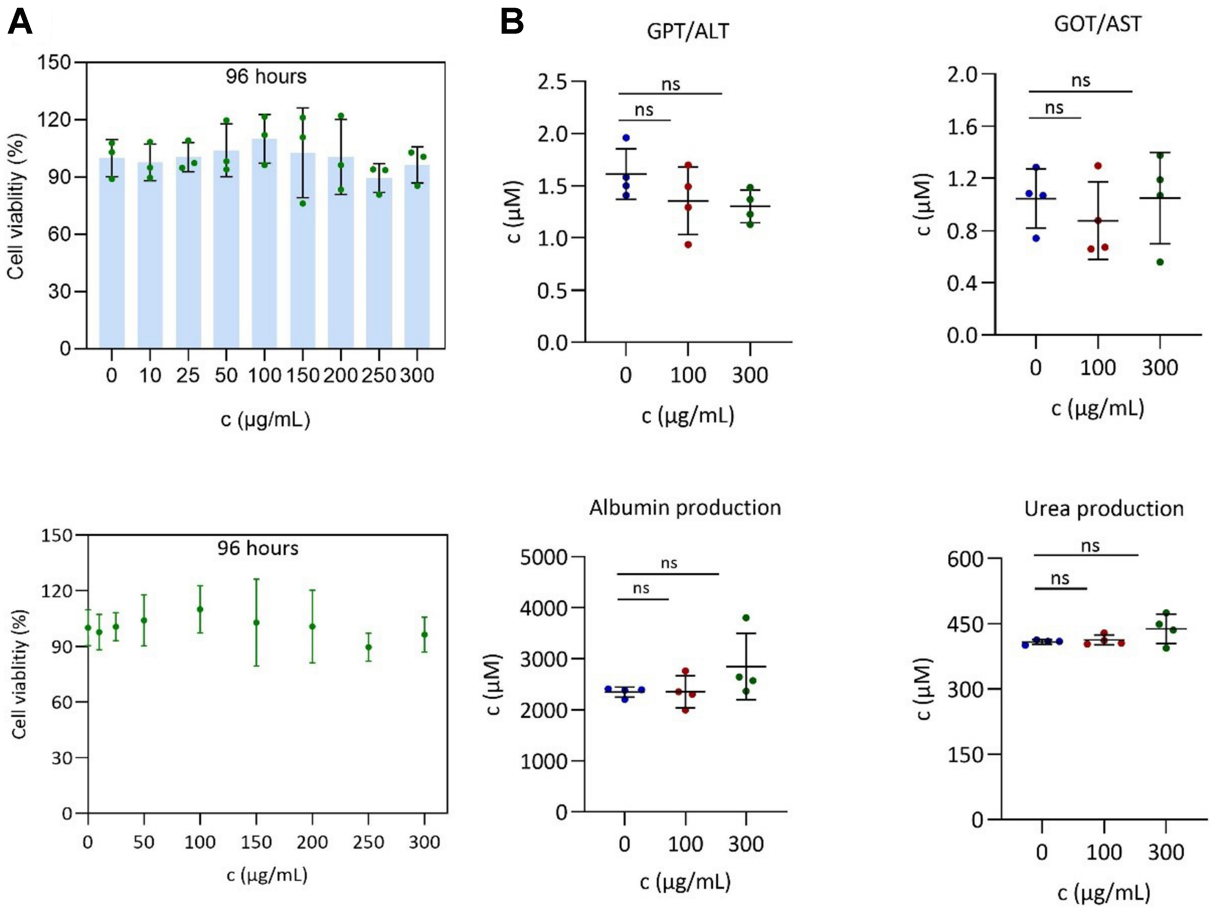

Figure 4. Liver organoid-based assessment of MOF ZIF-8 biocompatibility. (A) Cell viability determination using the standard CellTiter-Glo® luminescent assay, which quantifies ATP as a key indicator of cell health, and (B) liver function testing of hepatic organoids at 96 h after exposure to increasing concentrations of ZIF-8. No apparent dose-dependent reduction in viability was observed, and the IC_{50} was not reached within the tested concentration range (0-300 μg/mL). For panel A, statistical analyses across the nine concentration groups were performed using ordinary one-way ANOVA followed by Dunnett's multiple comparisons test, with the untreated group (0 μg/mL) serving as the control. For panel B, statistical analyses involving three groups were performed using ordinary one-way ANOVA followed by Dunnett's multiple comparisons test, with the untreated group serving as the control. "ns" indicates not significant ($P > 0.05$). Error bars represent the standard deviation. Data are presented as mean ± SD ($n = 3$ biological replicates). MOF: Metal–organic framework; ZIF-8: zeolitic imidazolate framework-8; ATP: adenosine triphosphate; ANOVA: analysis of variance; SD: standard deviation; GPT/ALT: alanine aminotransferase; GOT/AST: aspartate aminotransferase.

During the evaluation, ZIF-8 nanomaterials were administered via Matrigel embedding, enabling sustained and direct exposure to liver organoids. While the exact cellular uptake mechanisms remain to be elucidated, the porous structure of Matrigel allows diffusion of small molecules and minimizes selective retention of particulate materials. Compared with conventional 2D cell-based assays, our 3D liver organoid platform demonstrated higher tolerance to ZIF-8, with no detectable hepatotoxicity up to 300 μg/mL over 96 h. In contrast, previous studies [Table 2] using HepG2 or HeLa cells have reported dose-dependent cytotoxicity at lower concentrations (typically above 50-100 μg/mL), often associated with oxidative stress and membrane damage[38,44,45]. Although some organoid-based studies have explored MOF toxicity, many rely on less mature or structurally simplified systems and report toxicity at comparable or lower concentrations[33,38]. To our knowledge, this work represents one of the first studies employing functionally mature, hepatocyte-like liver organoids with comprehensive readouts for controlled evaluation of MOF nanotoxicity.

Table 2. Comparison of representative studies on MOF biocompatibility across experimental platforms

Study/source	Model system	MOF type	Exposure	Conc. range	Endpoints assessed	Observed biological response	Key findings	Relevance
This study (2026)	Liver organoid	ZIF-8	96 h	0-300 μg/mL	Viability, H&E, ALT, AST, urea, albumin	No detectable toxicity	First ZIF-8 evaluation in mature liver organoids	Programmable organoid evaluation platform
Mi *et al.*, (2022) [45]	HepG2 (2D hepatoma line)	ZIF-8 (DHM-loaded)	12-72 h	10-100 μg/mL	Viability, ROS, MMP, apoptosis markers	Dose-dependent cytotoxicity ≥ 50 μg/mL	Apoptosis observed on HepG2 cells	Static 2D toxicity model
Yang *et al.*, (2025) [19]	Caco-2 cells	Kaempferol-loaded ZIF-8	24 h	5-100 μg/mL	Cell viability	Cell viability remains above 80% at 100 μg/mL	ZIF-8 serves as the carrier for kaempferol delivery	Nanocarrier biocompatibility
Jarai *et al.*, (2020) [44]	HeLa cells	UiO-66 MOF	24 h	1-100 μg/mL	Viability, morphology	Dose-dependent toxicity > 25 μg/mL	General UiO-66 cytotoxicity screening	Conventional 2D toxicity screening
Li *et al.*, (2024) [38]	Intestine and hepatocyte organoid models	ZIF-8, ZIF-67, MIL-125	48 h	10-200 μg/mL	Viability, oxidative stress, DNA damage	Moderate toxicity at > 100 μg/mL	Patient-derived organoid evaluation	Early organoid-based evaluation
Shinozawa *et al.*, (2021) [35]	Liver organoid (for DILI)	Drugs (not MOFs)*	7 days	NA	GPT/ALT, bile canaliculi, omics	Organotypic response detected	High-fidelity DILI organoid model	High-fidelity organoid toxicity model

*Included as a representative example of a mature liver organoid toxicity evaluation rather than an MOF study. Exposure indicates exposure duration. MOF: Metal–organic framework; ZIF-8: zeolitic imidazolate framework-8; H&E: hematoxylin and eosin; GPT/ALT: alanine aminotransferase; GOT/AST: aspartate aminotransferase; ROS: reactive oxygen species; MMP: mitochondrial membrane potential; DILI: drug-induced liver injury; NA: not applicable.

Although the present study experimentally investigated only ZIF-8, comparison with previous studies involving UiO-66, ZIF-67, and MIL-125 MOFs highlights the substantial influence of framework chemistry, degradation behavior, and biological model on observed biocompatibility. Collectively, these findings indicate that MOF biocompatibility cannot be generalized across different framework families and underscore the need for systematic evaluation of diverse MOF materials using physiologically relevant organoid platforms.

Beyond conventional nanotoxicity evaluation, the rationale for assessing MOF safety extends to emerging applications in organoid and OOC bioengineering. As illustrated in Figure 5, MOFs are expected to play dual roles: first, as nanocarriers for drug delivery, which require rigorous safety validation, and second, as functional components within engineered organoid and OOC systems. In this latter context, MOFs may serve not only as nanoscale building blocks for localized therapeutic delivery, but also as nano-engineered regulators of organoid microenvironments capable of modulating biochemical gradients, mechanical properties, and physicochemical cues within 3D tissues. Such capabilities are central to the development of potentially programmable organoid systems[28]. The intrinsic modularity, tunable porosity, and stimuli-responsive behavior of MOFs distinguish them from passive biomaterials and position them as promising programmable nano–bio interfaces for future organoid engineering. Unlike conventional scaffold materials, MOFs may dynamically regulate biochemical gradients, release kinetics, and local microenvironmental conditions in a spatiotemporally controlled manner, thereby enabling future organoid systems with dynamically tunable microenvironments[46].

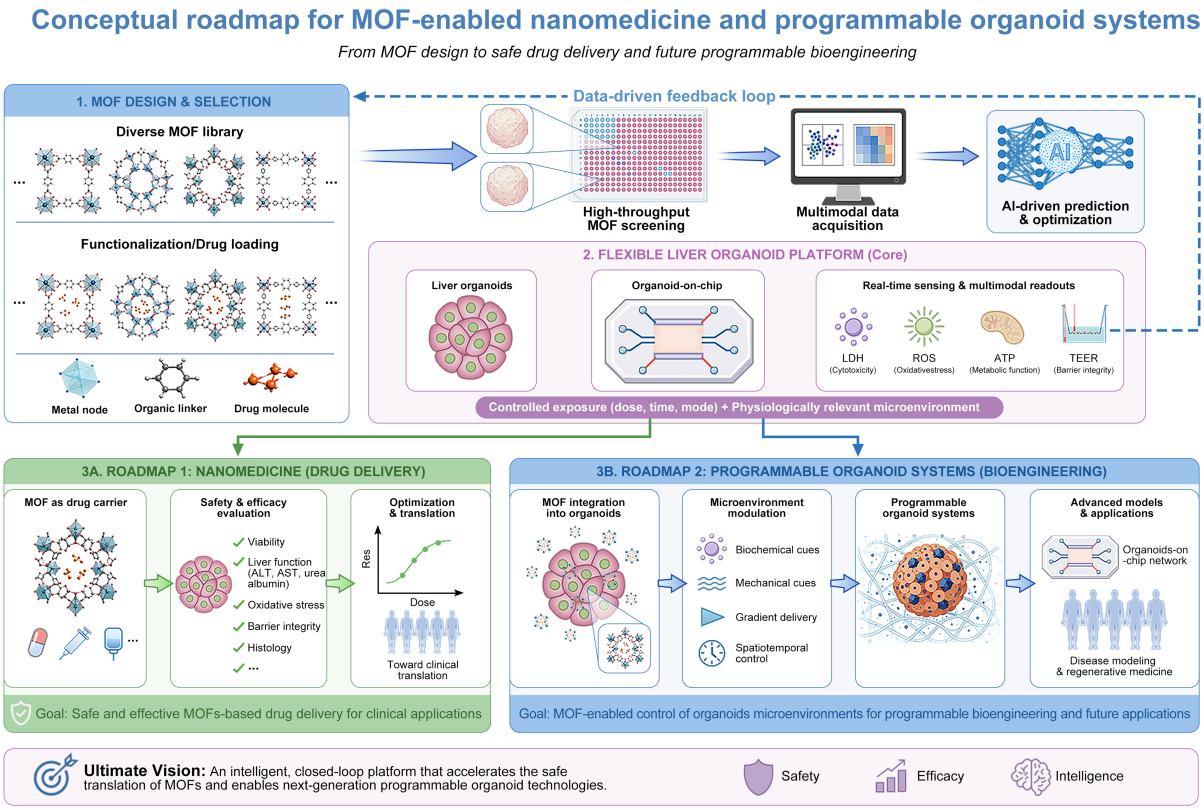

Figure 5. Conceptual roadmap for future MOF-enabled nanomedicine and organoid-based bioengineering systems. A closed-loop translational pipeline integrating organoid platforms, OOC technologies, and AI-driven modeling to support systematic MOF evaluation and design, supporting both safe MOF-based drug delivery and the emerging integration into organoid-based structured bioengineering systems. MOF: Metal–organic framework; OOC: organoid-on-chips; AI: artificial intelligence; LDH: lactate dehydrogenase; ROS: reactive oxygen species; ATP: adenosine triphosphate; TEER: transepithelial electrical resistance; ALT: alanine aminotransferase; AST: aspartate aminotransferase.

Such programmable nano–bio interfaces may ultimately support adaptive and self-regulating organoid systems for next-generation biomedical applications.

However, integrating nanomaterials into organoid architectures requires careful validation of their biocompatibility within complex multicellular environments. Organoids differ fundamentally from 2D systems in terms of prolonged exposure, spatial heterogeneity, and dynamic cell–cell interactions, all of which may influence nanomaterial behavior and toxicity. Therefore, demonstrating minimal toxicity of MOFs such as ZIF-8 in liver organoids represents a critical prerequisite for their future application in organoid-based bioengineering and bioconstruction. Although the direct incorporation of MOFs into flexible and potentially programmable organoid systems remains at a very early stage, the present study provides an essential safety foundation for such developments.

Despite these encouraging results, several limitations remain. The study focuses on short-term exposure and does not address potential long-term or cumulative effects. In addition, the monoculture liver organoid model lacks immune and vascular components, which are important for nanoparticle clearance, inflammatory responses, and systemic interactions. Addressing these limitations through more complex and integrated models will be necessary to further enhance physiological relevance and predictive power[47]. Furthermore, only one representative MOF (ZIF-8, ~200 nm) and a single organoid model were experimentally investigated. Because MOF biocompatibility depends strongly on framework chemistry,

metal composition, particle size, degradation behavior, surface properties, and biological context, the present findings should not be generalized to other MOF families. Systematic comparative evaluation of diverse MOF materials using physiologically relevant organoid platforms will therefore be essential for establishing the broader applicability of the proposed assessment framework. Although hepatic maturation was supported by molecular and functional analyses, additional characterization of CYP enzyme activity, hepatic transporters, and bile canaliculi formation was not performed and warrants further investigation in future studies. Moreover, mechanistic toxicity endpoints, including oxidative stress, mitochondrial dysfunction, endoplasmic reticulum stress, apoptosis, and longer-term exposure, were not evaluated and therefore remain important areas for future investigation. In addition, physicochemical characterization of ZIF-8 under the specific organoid exposure conditions, including surface charge, colloidal stability, release kinetics, degradation behavior, potential Zn^{2+} ion release, and post-exposure morphological changes in culture medium and Matrigel, was not investigated in the present study. Such analyses would provide valuable mechanistic insights into MOF–organoid interactions and may help interpret nanomaterial transport and exposure behavior. Additionally, the localization, cellular uptake, intracellular trafficking, retention, and degradation of ZIF-8 within the organoid–Matrigel system were not directly assessed and therefore also remain subjects for future investigation.

To place the present findings in a broader translational context, Figure 5 presents a conceptual roadmap outlining potential future directions for extending the proposed organoid-based biocompatibility evaluation framework. Building upon the present proof-of-concept study, future investigations may adopt a multi-tiered, data-driven, and platform-oriented strategy to further advance MOF evaluation and translational application. Future studies involving additional MOF classes, particle sizes, surface chemistries, organoid systems, and longer exposure durations, together with mechanistic investigations of MOF release, transport, cellular uptake, and degradation behavior, will be necessary to further establish the broader applicability of this framework. First, liver organoids can be integrated into high-throughput screening pipelines for drug-induced liver injury (DILI) and nanotoxicity assessment, enabling systematic evaluation of large MOF libraries and MOF–drug formulations while improving prediction of patient-specific toxicity responses that remain difficult to detect during the preclinical phase[47]. Second, incorporation of OOC systems and real-time biosensing technologies may enable dynamically controlled and physiologically relevant assessments by introducing fluid flow, mechanical stimulation, and multicellular interactions[48]. Such integrated platforms may further support real-time monitoring, adaptive feedback regulation, and closed-loop evaluation of MOF-enabled organoid systems. Third, multimodal datasets - including molecular design parameters, biochemical assays, imaging analyses, and biosensor-derived functional readouts - can be integrated to construct structure–toxicity and structure–function relationship databases, supporting quantitative modeling and artificial intelligence (AI)-driven prediction for the rational design and optimization of MOF-based bioengineering systems[49,50]. Collectively, these future directions outline a conceptual roadmap for extending the present organoid-based biocompatibility evaluation framework toward programmable organoid bioengineering and precision nanomedicine applications[51].

Collectively, this proof-of-concept study establishes an initial organoid-based framework for evaluating ZIF-8 biocompatibility and provides a foundation for future investigations involving additional MOF systems and organoid platforms. When integrated with OOC technologies, embedded biosensor systems, and AI-driven analytical platforms, such organoid-based frameworks may enable closed-loop and data-driven approaches for predictive toxicology and rational nanomaterial design. Beyond advancing the safe development of MOF-based nanomedicines, this work also establishes a foundational safety evaluation framework supporting the future convergence of MOFs, organoids, OOC technologies, biosensing, and AI-driven bioengineering toward adaptive and programmable living systems.

DECLARATIONS

Acknowledgments

The authors are deeply grateful to Prof. Lei Sun from the School of Science, Westlake University, for his critical review of this manuscript and invaluable insights on MOF nanomaterials.

Authors' contributions

Writing - original draft, methodology, investigation, data curation, conceptualization, funding acquisition: Bian, S.
Writing - original draft, methodology, data curation: Liu, S.
Writing - original draft: Chi, H.
Writing - review and editing, methodology: Chen, L.
Writing - review and editing: Tan, S.
Writing - original draft, methodology, project administration: Jiang, N.
Writing - review and editing, conceptualization: Vankelecom, H.
Methodology, conceptualization, funding acquisition: Zhang, X.
Writing - review and editing, supervision, project administration, funding acquisition, conceptualization: Li, C.

Availability of data and materials

The data supporting the findings of this study are available from the corresponding authors upon reasonable request.

AI and AI-assisted tools statement

Not applicable.

Financial support and sponsorship

This work was supported by the Shenzhen Medical Research Fund (Project No. D250402001), the National Natural Science Foundation of China (NSFC) (Grant No. 82104122) and the NSFC Foreign Scholars Project (Grant No. W2531016), and the Peacock Team Project (No. KQTD20240729102029016), the Shenzhen Longgang District Key Laboratory of Intelligent Biophotonics and Brain Disease Diagnosis and Treatment, Guangdong Basic Research Center of Excellence for Aggregate Science.

Conflicts of interest

Bian, S. and Li, C. are the Guest Editors of the Special Topic "*Flexible and Programmable Reconstruction of Organoids and Organoid-on-Chips*" in *Soft Science*. They had no involvement in the review or editorial process of this manuscript, including but not limited to reviewer selection, evaluation, or the final decision, while the other authors have declared that they have no conflicts of interest.

Ethical approval and consent to participate

This study used commercially available human embryonic stem cell-derived hepatic progenitor organoids (hESCs; H1, Cat No: CL-0889, Wuhan Procell Biotechnology) and did not involve the recruitment of human participants, collection of human samples, identifiable personal information, or animal experiments. Commercially available de-identified Single Donor Human Serum Off the Clot and Single Donor Human Urine (Innovative Research, Shanghai, China) were used solely as reference controls for liver function assays and did not involve human subject recruitment. According to Article 32 of the Measures for the Ethical Review of Life Science and Medical Research Involving Human Subjects (Trial), this study meets the conditions for exemption from ethical review.

Consent for publication

Not applicable.

Copyright

The Author(s) 2026.

REFERENCES

1. Ding, M.; Flaig, R. W.; Jiang, H. L.; Yaghi, O. M. Carbon capture and conversion using metal-organic frameworks and MOF-based materials. *Chem. Soc. Rev.* **2019**, *48*, 2783-828. DOI PubMed
2. Rubio-Martinez, M.; Avci-Camur, C.; Thornton, A. W.; Imaz, I.; Maspoch, D.; Hill, M. R. New synthetic routes towards MOF production at scale. *Chem. Soc. Rev.* **2017**, *46*, 3453-80. DOI PubMed
3. Furukawa, H.; Cordova, K. E.; O'Keeffe, M.; Yaghi, O. M. The chemistry and applications of metal-organic frameworks. *Science* **2013**, *341*, 1230444. DOI PubMed
4. Cai, G.; Yan, P.; Zhang, L.; Zhou, H. C.; Jiang, H. L. Metal-organic framework-based hierarchically porous materials: synthesis and applications. *Chem. Rev.* **2021**, *121*, 12278-326. DOI PubMed
5. Fan, X.; Zhang, X.; Li, L.; Cao, M. Recent progress and perspective of microwave absorption materials derived from metal-organic frameworks. *Soft. Sci.* **2024**, *4*, 43. DOI
6. Shivanna, M.; Yang, Q. Y.; Bajpai, A.; Patyk-Kazmierczak, E.; Zaworotko, M. J. A dynamic and multi-responsive porous flexible metal-organic material. *Nat. Commun.* **2018**, *9*, 3080. DOI PubMed PMC
7. Yaghi, O. M.; O'Keeffe, M.; Ockwig, N. W.; Chae, H. K.; Eddaoudi, M.; Kim, J. Reticular synthesis and the design of new materials. *Nature* **2003**, *423*, 705-14. DOI PubMed
8. Gong, W.; Chen, Z.; Dong, J.; Liu, Y.; Cui, Y. Chiral metal-organic frameworks. *Chem. Rev.* **2022**, *122*, 9078-144. DOI PubMed
9. Xu, L.; Yu, H.; Li, X.; Ge, J. Biomacromolecule-MOF composites for intracellular delivery: from empirical construction to rational design and AI-assisted screening. *Small* **2026**, e74697. DOI PubMed
10. Wu, M. X.; Yang, Y. W. Metal-organic framework (MOF)-based drug/cargo delivery and cancer therapy. *Adv. Mater.* **2017**, *29*, 1606134. DOI PubMed
11. Wang, S.; Fu, Y.; Wang, T.; et al. Fabrication of robust and cost-efficient Hoffmann-type MOF sensors for room temperature ammonia detection. *Nat. Commun.* **2023**, *14*, 7261. DOI PubMed PMC
12. Hao, R.; He, F.; Gao, X.; et al. Prussian blue analogue-decorated Ni-MOF composite for ultrasensitive electrochemical detection of myricetin. *Electrochim. Acta.* **2026**, *558*, 148525. DOI
13. Ding, M.; Liu, W.; Gref, R. Nanoscale MOFs: from synthesis to drug delivery and theranostics applications. *Adv. Drug. Deliv. Rev.* **2022**, *190*, 114496. DOI PubMed
14. Della Rocca, J.; Liu, D.; Lin, W. Nanoscale metal-organic frameworks for biomedical imaging and drug delivery. *Acc. Chem. Res.* **2011**, *44*, 957-68. DOI PubMed PMC
15. Sun, Z.; Li, T.; Mei, T.; et al. Nanoscale MOFs in nanomedicine applications: from drug delivery to therapeutic agents. *J. Mater. Chem. B.* **2023**, *11*, 3273-94. DOI PubMed
16. Lu, K.; Aung, T.; Guo, N.; Weichselbaum, R.; Lin, W. Nanoscale metal-organic frameworks for therapeutic, imaging, and sensing applications. *Adv. Mater.* **2018**, *30*, e1707634. DOI PubMed PMC
17. Park, J.; Jiang, Q.; Feng, D.; Mao, L.; Zhou, H. C. Size-controlled synthesis of porphyrinic metal-organic framework and functionalization for targeted photodynamic therapy. *J. Am. Chem. Soc.* **2016**, *138*, 3518-25. DOI PubMed
18. Zhao, H.; Shu, G.; Zhu, J.; Fu, Y.; Gu, Z.; Yang, D. Persistent luminescent metal-organic frameworks with long-lasting near infrared emission for tumor site activated imaging and drug delivery. *Biomaterials* **2019**, *217*, 119332. DOI PubMed
19. Yang, G.; Wang, J.; Wang, R.; et al. Zeolitic imidazolate framework-8 (ZIF-8) as a carrier for kaempferol delivery to protect against gamma radiation-induced mortality and damage. *Pharmaceutics* **2025**, *17*, 1489. DOI PubMed PMC
20. Niu, L.; Zeng, L.; Yu, D.; Cheng, S.; Feng, G. Overscreening-driven modulation of ion adsorption and desorption in conductive MOF electrodes by charging rates. *ACS. Nano.* **2025**, *19*, 2581-90. DOI PubMed
21. He, R.; He, J.; Shen, J.; Fu, H.; Zhang, Y.; Wang, B. Recent advances in multifaceted applications of MOF-based hydrogels. *Soft. Sci.* **2024**, *4*, 37. DOI
22. Wu, Y. N.; Zhou, M.; Li, S.; et al. Magnetic metal-organic frameworks: γ-Fe_2O_3@MOFs via confined in situ pyrolysis method for drug delivery. *Small* **2014**, *10*, 2927-36. DOI PubMed
23. Wang, Y.; Yan, J.; Wen, N.; et al. Metal-organic frameworks for stimuli-responsive drug delivery. *Biomaterials* **2020**, *230*, 119619. DOI PubMed
24. Liu, Y.; Zhao, Y.; Chen, X. Bioengineering of metal-organic frameworks for nanomedicine. *Theranostics* **2019**, *9*, 3122-33. DOI PubMed PMC
25. Obeso, J. L.; Huxley, M. T.; Leyva, C.; et al. The role of dynamic metal-ligand bonds in metal-organic framework chemistry. *Coord. Chem. Rev.* **2023**, *496*, 215403. DOI
26. Yi, S. A.; Zhang, Y.; Rathnam, C.; Pongkulapa, T.; Lee, K. B. Bioengineering approaches for the advanced organoid research. *Adv. Mater.* **2021**, *33*, e2007949. DOI PubMed PMC

27. Kang, M.; Cho, Y.; Kim, T. Metal- and covalent-organic framework-based drug delivery systems: applications to control cell functions. *Coord. Chem. Rev.* **2025**, *527*, 216400. DOI
28. Brassard, J. A.; Lutolf, M. P. Engineering stem cell self-organization to build better organoids. *Cell. Stem. Cell.* **2019**, *24*, 860-76. DOI PubMed
29. Ettlinger, R.; Lächelt, U.; Gref, R.; et al. Toxicity of metal-organic framework nanoparticles: from essential analyses to potential applications. *Chem. Soc. Rev.* **2022**, *51*, 464-84. DOI PubMed PMC
30. He, W.; Sun, Q.; Ge, D.; Liu, Y.; Sun, B. Application of nanomaterials in organoid culture and cryopreservation. *Nanoscale. Adv.* **2025**, *7*, 7483-503. DOI PubMed PMC
31. Zhu, W.; Guo, J.; Agola, J. O.; et al. Metal-organic framework nanoparticle-assisted cryopreservation of red blood cells. *J. Am. Chem. Soc.* **2019**, *141*, 7789-96. DOI PubMed
32. Brooks, A.; Liang, X.; Zhang, Y.; et al. Liver organoid as a 3D *in vitro* model for drug validation and toxicity assessment. *Pharmacol. Res.* **2021**, *169*, 105608. DOI PubMed
33. Zhang, C. J.; Meyer, S. R.; O'Meara, M. J.; et al. A human liver organoid screening platform for DILI risk prediction. *J. Hepatol.* **2023**, *78*, 998-1006. DOI PubMed PMC
34. Choi, S. Y.; Kim, T. H.; Kim, M. J.; et al. Validating well-functioning hepatic organoids for toxicity evaluation. *Toxics* **2024**, *12*, 371. DOI PubMed PMC
35. Shinozawa, T.; Kimura, M.; Cai, Y.; et al. High-fidelity drug-induced liver injury screen using human pluripotent stem cell-derived organoids. *Gastroenterology* **2021**, *160*, 831-46.e10. DOI PubMed PMC
36. Zhang, H.; Huang, N.; Bian, S.; Sawan, M. Brain organoids-on-chip for neural diseases modeling: history, challenges and trends. *J. Pharm. Anal.* **2025**, *15*, 101323. DOI PubMed PMC
37. Wu, X.; Wu, M. A.; Zou, J.; Kleinstreuer, N.; Wu, J. C. Reimagining human-centric drug development with new approach methodologies. *Science* **2026**, *392*, 371-8. DOI PubMed PMC
38. Li, D.; Zhang, R.; Le, Y.; et al. Organoid-based assessment of metal-organic framework (MOF) nanomedicines for *ex vivo* cancer therapy. *ACS. Appl. Mater. Interfaces.* **2024**, *16*, 33070-80. DOI PubMed
39. Roudaut, M.; Caillaud, A.; Souguir, Z.; et al. Human induced pluripotent stem cells-derived liver organoids grown on a Biomimesys® hyaluronic acid-based hydroscaffold as a new model for studying human lipoprotein metabolism. *Bioeng. Transl. Med.* **2024**, *9*, e10659. DOI PubMed PMC
40. Shah, P.; Zhu, X.; Zhang, X.; He, J.; Li, C. Z. Microelectromechanical system-based sensing arrays for comparative in vitro nanotoxicity assessment at single cell and small cell-population using electrochemical impedance spectroscopy. *ACS. Appl. Mater. Interfaces.* **2016**, *8*, 5804-12. DOI PubMed
41. Zhang, H.; Huang, N.; Bian, S.; Sawan, M. Platinum wire-embedded culturing device for interior signal recording from lollipop-shaped neural spheroids. *Cyborg. Bionic. Syst.* **2025**, *6*, 0220. DOI PubMed PMC
42. Zhang, X.; Li, Y.; Van Goethem, C.; et al. Electrochemically assisted interfacial growth of MOF membranes. *Matter* **2019**, *1*, 1285-92. DOI
43. Kim, H.; Im, I.; Jeon, J. S.; et al. Development of human pluripotent stem cell-derived hepatic organoids as an alternative model for drug safety assessment. *Biomaterials* **2022**, *286*, 121575. DOI PubMed
44. Jarai, B. M.; Stillman, Z.; Attia, L.; Decker, G. E.; Bloch, E. D.; Fromen, C. A. Evaluating UiO-66 metal-organic framework nanoparticles as acid-sensitive carriers for pulmonary drug delivery applications. *ACS. Appl. Mater. Interfaces.* **2020**, *12*, 38989-9004. DOI PubMed PMC
45. Mi, X.; Lu, J.; Dong, M.; Lou, Y.; Zhan, X.; Chen, X. Pro-apoptotic effect of zeolitic imidazolate framework-8 (ZIF-8)-loaded dihydromyricetin on HepG2 cells. *Molecules* **2022**, *27*, 5484. DOI PubMed PMC
46. Gjorevski, N.; Nikolaev, M.; Brown, T. E.; et al. Tissue geometry drives deterministic organoid patterning. *Science* **2022**, *375*, eaaw9021. DOI PubMed PMC
47. Andersson-Rolf, A.; Clevers, H. New developments and applications of human organoids. *Nat. Rev. Mol. Cell. Biol.* **2026**, *27*, 543-58. DOI PubMed
48. Jin, Y.; Park, S.; Cho, S. Organoid analytical toolkits. *Nat. Rev. Bioeng.* **2026**, *4*, 336-52. DOI
49. Tan, S.; Ding, Y.; Wang, W.; et al. Development of an AI model for DILI-level prediction using liver organoid brightfield images. *Commun. Biol.* **2025**, *8*, 886. DOI PubMed PMC
50. Bai, C.; Wu, L.; Li, R.; Cao, Y.; He, S.; Bo, X. Machine learning-enabled drug-induced toxicity prediction. *Adv. Sci.* **2025**, *12*, e2413405. DOI PubMed PMC
51. Liu, W.; Pang, P. D.; Wu, C. A.; Tagle, D.; Wu, J. C. New approach methodologies for drug discovery. *Cell* **2026**, *189*, 1877-903. DOI PubMed PMC

Disclaimer/Publisher's Note: All statements, opinions, and data contained in this publication are solely those of the individual author(s) and contributor(s) and do not necessarily reflect those of OAE and/or the editor(s). OAE and/or the editor(s) disclaim any responsibility for harm to persons or property resulting from the use of any ideas, methods, instructions, or products mentioned in the content.

© The Author(s) 2026. Open Access This article is licensed under a Creative Commons Attribution 4.0 International License (https://creativecommons.org/licenses/by/4.0/), which permits unrestricted use, sharing, adaptation, distribution and reproduction in any medium or format, for any purpose, even commercially, as long as you give appropriate credit to the original author(s) and the source, provide a link to the Creative Commons license, and indicate if changes were made.